Effects of Crystalline Microstructure on Oil Migration in a Semisolid Fat Matrix

ARTICLE *in* CRYSTAL GROWTH & DESIGN · JULY 2004

Impact Factor: 4.89 · DOI: 10.1021/cg049933n

6 AUTHORS, INCLUDING:

Juliana Ract
University of São Paulo
17 PUBLICATIONS **155** CITATIONS
SEE PROFILE

Luiz Antonio Gioielli
University of São Paulo
126 PUBLICATIONS **988** CITATIONS
SEE PROFILE

Alejandro Gregorio Marangoni
University of Guelph
344 PUBLICATIONS **6,891** CITATIONS
SEE PROFILE

CRYSTAL GROWTH & DESIGN
2004
VOL. 4, NO. 4
731−736

Effects of Crystalline Microstructure on Oil Migration in a Semisolid Fat Matrix

Elena Dibildox-Alvarado,[†] Juliana Neves Rodrigues,[‡] Luiz Antonio Gioielli,[‡] Jorge F. Toro-Vazquez,[†] and Alejandro G. Marangoni*[,§]

Facultad de Ciencias Químicas, Universidad Autónoma de San Luis Potosí, Av. Dr. Manuel Nava No. 6, Zona Universitaria, C.P. 78210, San Luis Potosí, S.L.P. México, Faculty of Pharmaceutical Sciences, Universidade de São Paulo, Av. Prof. Lineu Prestes 580, 05508-900, São Paulo, Brazil, and Department of Food Science, University of Guelph, Guelph, ON N1G2W1, Canada

Received February 16, 2004; Revised Manuscript Received March 31, 2004

Ⓦ **This paper contains enhanced objects available on the Internet at http://pubs.acs.org/crystal.**

ABSTRACT: Oil migration from a 60:40 (w/w) mixture of peanut oil and chemically interesterified and hydrogenated palm oil (IHPO) was a strong function of the cooling rate experienced by the fat mixture during crystallization, namely, 0.4, 1.2, and 6.0 °C/min. The relative oil loss determined gravimetrically was inversely proportional to the cooling rate. Oil loss was also inversely related to the storage modulus (G′) and the yield force of the fat. After 1 day storage at 20 °C, the start of the oil loss studies, the composition and polymorphism of the fat crystals crystallized at different rates were similar, as judged by differential scanning calorimetry and powder X-ray diffraction. Crystals were in the same β' modification and had similar peak melting temperatures. Microstructure, on the other hand, was profoundly affected by the cooling rate: average crystal size decreased from 8.2 μm (at 0.4 °C/min) to 3.9 μm (at 6.0 °C/min). Using Darcy's Law, it was possible to calculate permeability coefficients using the structural parameters obtained in this work. Decreases in permeability coefficient as a function of increasing cooling rate were mainly related to decreases in crystal size.

Introduction

The capacity of a fat crystal network to trap oil is an important material property that directly influences oil migration. In many composite confectionery products, a chocolate layer is usually in direct contact with a fat-based cream. These creams contain large amounts of highly mobile oils, such as peanut or hazelnut oils. This oil has a tendency to migrate into the chocolate layer, leading to bloom formation and softening of the chocolate, as well as hardening of the cream layer.[1,2] Recent work in this area has focused on the measurement of oil migration into chocolate, mainly using magnetic resonance imaging.[3−5] Several other methods have been successfully used in the measurement of oil migration.[2] On the other hand, very little work, if any, has been directed toward defining the structural factors in a fat that influence the ability of a fat crystal network to bind liquid oil.

Fats are structured as a network of fat crystals, usually crystal aggregates, with liquid oil trapped within.[6−8] It is the purpose of this work to define the relative effects of solid fat content (SFC), crystal size, solid-state composition and polymorphism, crystal microstructure, as well as material elasticity and hardness, on oil migration through a semisolid crystalline fat matrix.

Materials and Methods

Sample Preparation and Treatments. Peanut oil and chemically interesterified, hydrogenated palm oil (IHPO) were blended at a ratio of 60:40 (w/w). IHPO was used as a generic hardstock, and its properties have been previously reported.[9] IHPO was melted at 80 °C for 30 min, thoroughly mixed with the peanut oil and poured into aluminum cylindrical molds connected to a Neslab RTE-111 (Fisher Scientific, St. Louis, MO) controlled rate water bath (Figure 1). The blends were crystallized into 20-mm diameter and 3.2-mm thickness cylinders at three different cooling rates, 0.4, 1.2, and 6.0 °C/min. The two lowest cooling rates were within the cooling capabilities of the water bath, while the fastest cooling rate was achieved by precooling the molds to 5 °C and introducing the 80 °C molten fat directly into the precooled molds. Cooling rates were determined from direct temperature measurements of the crystallizing material using a Fluke 51 K/J thermocouple thermometer (Fisher Scientific, St. Louis, MO). Samples were removed from the molds once they appeared solid using a plastic plunger of the same dimensions as the sample. These $t = 0$ samples are referred to as "0" in the figures. All samples were initially stored at 20 °C on aluminum foil for 24 h. These $t = 1$ day samples are referred to as "1" in the figures. After this initial storage period, four different treatments were applied to the samples: (T1) crystallized samples were kept on aluminum foil at 20 °C for 3 days; (T2) crystallized samples were transferred onto filter papers and kept at 20 °C for 3 days; (T3) crystallized samples were transferred onto filter papers and the storage temperature was cycled between 20 and 25 °C (12 h at each temperature) for a period of 3 days; (T4) crystallized samples were transferred onto filter papers and the storage temperature cycled between 20 and 30 °C (12 h at each temperature) for 3 days. Treatment T1 is the control to which treatments T2, T3, and T4 should be compared.

All analyses were performed at the initial time ($t = 0$), when samples were initially removed from the molds, after 24 h of storage ($t = 1$ day), and at the end of the cycling/storage period ($t = 4$ days).

Oil Loss Determination. For characterizing oil migration, the amount of oil that each sample lost to filter papers (Whatman #4, 110-mm diameter) was determined by weighing filter papers before and after the treatments applied to the

* Corresponding author. Ph: (519) 824-4120 x54340. Fax: (519) 824-6631. E-mail: amarango@uoguelph.ca.
[†] Universidad Autónoma de San Luis Potosí.
[‡] Universidade de São Paulo.
[§] University of Guelph.

10.1021/cg049933n CCC: $27.50
Published on Web 05/08/2004

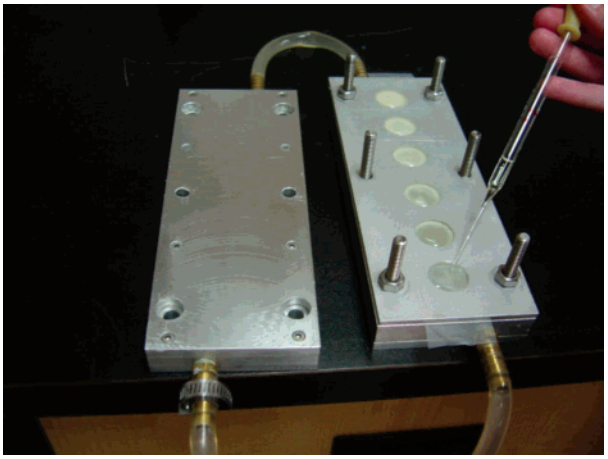

Figure 1. Aluminum molds used for the crystallization of the fat−oil mixtures at different cooling rates.

samples. Oil loss was then calculated as:

$$\text{oil loss} = \frac{\text{wt. paper } (t) - \text{wt. paper } (t = 0)}{\text{wt. disc } (t = 0)} \times 100\% \quad (1)$$

A "blank" filter paper was included in all experiments to account for the effects of the treatments on the paper itself. Five replicates were performed (five separate disks on individual filter papers) and the average and standard deviation were reported. Filter papers must be large enough so as not to become saturated prior to the end of the measurement period.

Differential Scanning Calorimetry. To examine the effects of the different cooling rates during crystallization on the melting behavior of the samples, differential scanning calorimetry (DSC) analysis was performed with a Q 1000 DSC (TA Instruments, Mississauga, ON, Canada). Nitrogen purge gas was used to prevent condensation in the cell and an empty pan was used as reference. A small piece (8−12 mg) was cut from the sample disks exposed to the different treatments, and hermetically sealed in aluminum pans. Pans were heated from 20 to 80 °C at a constant temperature ramp of 5 °C/min. Peak maxima and enthalpy of melt were determined. Three separate disks samples were analyzed and two samples from each disk were obtained from the region between the center of the disks and the outer edge (diametrically opposite from each other). Values reported are the averages of the three disks, which in turn are the average of the two samples per disk.

Solid Fat Content. SFC was measured by pulsed nuclear magnetic resonance (pNMR) with an MQ 20 NMR analyzer (Bruker, Milton, Canada). Samples were melted at 80 °C for 30 min to erase any crystal history. The melted fats were thoroughly mixed, placed in NMR tubes, and crystallized at 0.4, 1.2, and 6.0 °C/min to 20 °C ($t = 0$). In the first experiment, samples were stored for 1 day at 20 °C ($t = 1$). In the second experiment, samples crystallized to 20 °C at 0.4, 1.2, and 6.0 °C/min ($t = 0$) were incubated at 20 °C for 1 day ($t = 1$ day), and then transferred to 25 or 30 °C. After 12 h, the SFC of the samples stored at 25 and 30 °C was determined and samples were returned to 20 °C and stored for another 12 h. This process was repeated for 3 days ($t = 4$ days). Three replicates samples were analyzed at each cooling rate−time−temperature combination and the average and standard deviation was reported.

Small Deformation Rheology. Rheological measurements at small deformations were made using an AR 2000 rheometer (TA Instruments, Mississauga, ON, Canada) with a 2-cm flat plate attachment. The sample platform temperature was controlled, allowing for sample temperature to be maintained during analysis. Sample disk normal compression was set to 10% to ensure good contact between the parallel plate attachment and the fat sample. The storage (G′), loss (G″) and complex (G*) moduli as well as the tangent of the phase angle (tan δ) of the sample disks were determined within the linear viscoelastic region (LVR) by performing oscillatory stress sweeps from 5 to 500 Pa, at a constant frequency of 1 Hz. Three samples were analyzed at each treatment−cooling rate combination. The average and standard deviation are reported.

Large Deformation Rheology. Large deformation mechanical measurements (compression test between parallel plates) were made using a materials tester (SMS Materials Test, Texture analyzer model MT-LQ, Surrey, UK) with a 50 N load cell. Sample disks were compressed uniaxially at a crosshead speed of 5 mm/s until failure occurred. Sample temperature was maintained during compression by circulating cooled water through the base plate. The peak breaking force (N) was recorded. Three samples were analyzed at each treatment−cooling rate combination. The average and standard deviation are reported.

Powder X-ray Diffraction. A 1-mm-thick slab was cut with a scalpel from the sample disk and placed on a wire holder in the rotation center of the Huber Four-circle. The scans were taken with a single point Bicron detector at discrete 22 angular intervals. The lithium fluoride monochromator was set to select the Cu−Kα1 line of our sealed tube X-ray source, $\alpha = 0.154$ nm. The FWHM of the beam was 0.1 deg in 2θ. The X-ray generator unit is made by Enraf-Nonius.

Polarized Light Microscopy and Microanalysis. A small droplet (about 10 μL) of melted fat (80 °C for 30 min) was placed on a preheated (80 °C) glass slide, using a preheated capillary tube. A preheated glass cover slip was carefully placed over the sample to produce a film of uniform thickness. The slides were incubated for 10 min at 60 °C, crystallized at 0.4, 1.2, and 6 °C/min to 20 °C, and stored at this temperature for 24 h. Sample temperature was controlled Linkam LTS 350 hot/cold stage (Linkam Scientific Instruments Ltd., Surrey, England). When viewed by polarized light microscopy (PLM) (Olympus BH, Tokyo, Japan) the birefringent solid microstructural elements of the network could be directly observed and digital images were acquired via a Sony XC75 CCD camera and LG-3 capture board (Scion Corporation, Frederick, USA).

Grayscale images were then inverted, thresholded, and analyzed with a particle counting algorithm using NIH Image (National Institute of Health, Bethesda, USA) to determine a particle-counting fractal dimension, D_f. The algorithm works as follows: the number of distinct particles (N) is first counted within the entire image of known length (L). At 5% increments, the image is cropped to smaller lengths and the number of particles again is counted. This cropping and counting procedure is repeated until the length of the image is 35% of the original size. The slope of the linear regression of the log−log plot of the number of particles (N) within each region of length (L) corresponds to D_f. It is important to note that two counts are performed, one that includes particles touching the edges of each region of interest and one that excludes those at the edges. The average of the D_f values obtained by counts excluding and including particles at the edges best represents the spatial distribution of mass.

The noninverted, thresholded gray scale images were also analyzed using Benoit 1.3 (TruSoft International Inc., St. Petersburg, USA, http://www.trusoft-international.com) to determine the box-counting fractal dimension (D_b). In this method, a grid is laid over the image, and the number of boxes that are occupied by mass are counted. The size of the boxes that make up the grid is then iteratively reduced and the occupied boxes are counted. The number of occupied boxes (N) versus the length of the boxes that make up the grid (L) is plotted on log−log axes, and the slope corresponds to $-D_b$. Three separate slides were analyzed at each treatment−cooling rate combination. The average and standard deviation are reported.

Mean particle sizes were determined using image analysis toolkit plug-ins (Reindeer Graphics Inc., North Carolina, USA) for Adobe Photoshop 5.5 (Adobe Systems Inc., San Jose, USA). Calibration was performed by using the IP·Measure: Calibration filter using an image of a calibration micrometer. Mean

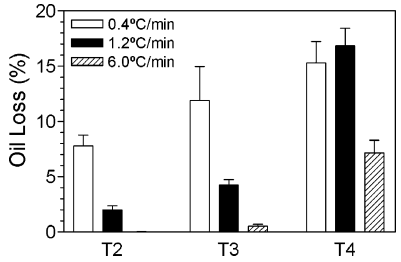

Figure 2. Oil loss (% w/w) from sample disks to filter paper.

particle sizes were obtained by using the IP·Features: Distribution filter with output on the basis of feature area. The program assumes a circular geometry and obtains the square root of the quotient of the area to π.

Results and Discussion

Oil loss from sample disks crystallized at the three different cooling rates are shown in Figure 2. In general, the lower the cooling rate used in the crystallization process, the greater the oil loss. Moreover, the 20 °C isothermal storage treatment (T2) displayed the lowest oil loss relative to the 20/25 °C (T3) and 20/30 °C (T4) cycling treatments. Thus, the higher the maximum temperature attained during cycling, the greater the oil loss. In what follows, we will try to explain the observed behavior.

Small deformation rheological measurements demonstrated that the higher the cooling rate used in the crystallization process, the higher the storage modulus (G′), as can be appreciated in Figure 3A. Exceptions to this generalization were observed in T3 and T4 (temperature cycling treatments), where the G′ of samples crystallized at 1.2 °C/min were either the same (T3), or lower (T4), than the G′ of samples crystallized at 0.4 °C/min. However, the G′ of samples crystallized at 6 °C/min were always higher than either of the other two, both for T3 and T4. A quick inspection of the patterns obtained reveals peculiarities in the sample crystallized at 0.4 °C, in which this sample seems to be relatively insensitive to temperature cycling and storage period. Cycling in general, as well as the maximum temperature attained during cycling, lead to a decrease in G′, indicative of a loss in structural integrity, induced by the greater oil loss in these samples (Figure 2). The same trends were observed for the loss (G″) and complex (G*) moduli (Figure 3B,C, respectively). On the other hand, tan δ was not sensitive to cooling rate-induced differences, but did increase upon temperature cycling, as well as for higher maximum temperatures attained during cycling (Figure 3D).

Large deformation measurements demonstrated that the yield force of samples crystallized at high cooling rates was greater than the yield force of samples crystallized at low cooling rates (Figure 4). Temperature cycling, as well as the maximum temperature attained during cycling lead to decreases in the yield force, indicative of a loss in structural integrity in the sample. This behavior was in agreement with the small deformation rheology results (Figure 3). No data are shown for samples crystallized at 0.4 °C/min, since they were too soft to measure.

To help determine the causes for the increase in elasticity, hardness, and the oil binding capacity in

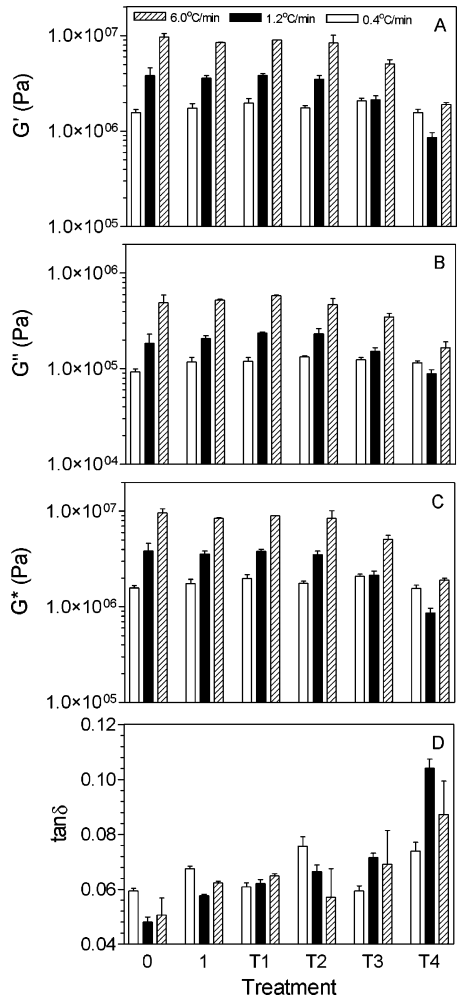

Figure 3. Variation in the (A) storage modulus (G′), (B) loss modulus (G″), (C) complex modulus (G*), and (D) tan δ as a function of cooling rate and temperature−time treatment.

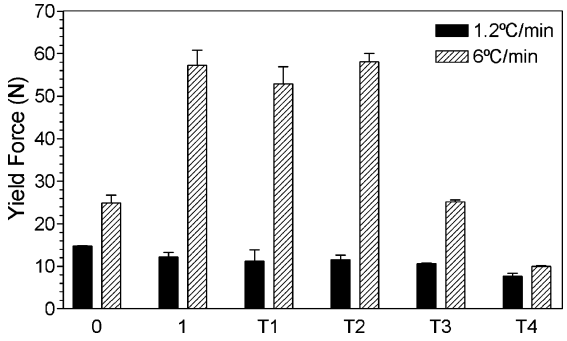

Figure 4. Variation in the yield force as a function of cooling rate and temperature−time treatment.

samples crystallized at higher cooling rates, a series of structural indicators were obtained. The solid fat content (SFC) of samples crystallized at 0.4 and 6 °C/min were lower ($P < 0.05$) than the SFC of samples crystallized at 1.2 °C/min immediately after the crystallization temperature was reached ($t = 0$, Figure 5). However, 1 day of storage at 20 °C, samples had stabilized and the SFC of samples crystallized at 1.2 and 6 °C/min were higher ($P < 0.05$) than the SFC of samples crystallized at 0.4 °C/min (Figure 5), but were not significantly different from each other ($P > 0.05$). When samples were exposed to higher temperatures during temperature

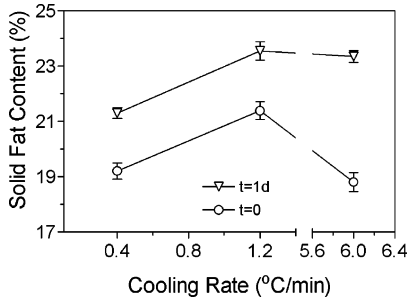

Figure 5. Changes in solid fat content (SFC) as a function of cooling rate for samples crystallized in glass NMR tubes at 20 °C, immediately after reaching 20 °C and after 1 day of storage at 20 °C.

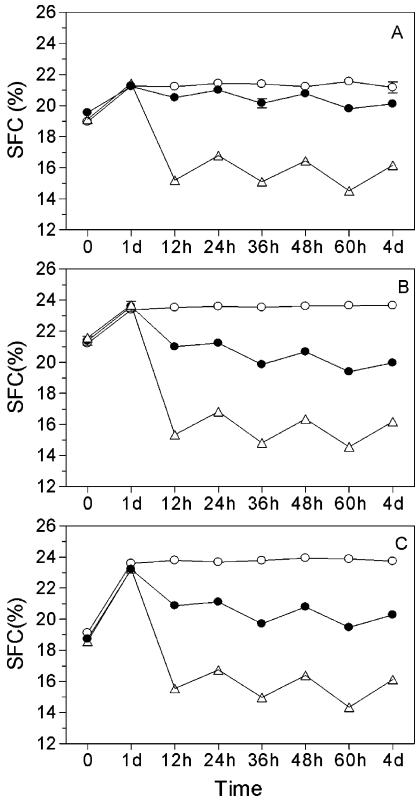

Figure 6. Changes in solid fat content (SFC) as a function of storage time for samples crystallized in glass NMR tubes at 20 °C at (A) 0.4 °C/min, (B) 1.2 °C/min, and (C) 6 °C/min. Samples were held at 20 °C for 1 day, and then either kept at this temperature, or transferred to 25 or 30 °C for 12 h. At the end of this period, samples were returned to 20 °C for 12 h. This process was repeated for 3 days.

cycling (Figure 6), the initial effect of cooling rate on SFC was erased, and the behavior of the samples was similar. Even though a reduction in SFC upon exposure to higher temperatures would in principle lead to a weakening of the fat crystal network and an increase in oil loss, SFC was definitely not the sole factor influencing oil loss. For example, exposure to higher temperatures erased the effects of cooling rate on SFC; however, cooling rate effects on oil loss (Figure 2) and rheological parameters (Figure 3) were evident under these conditions. Thus, SFC cannot be used as the sole predictor of oil loss and fat crystal network structural integrity.

Table 1. Melting Enthalpy (ΔH) and Peak Melting Temperature (T_m) for Samples Crystallized at Three Different Cooling Rates for the Different Time−Temperature Treatments[a]

	0	1	T1	T2	T3	T4
			6 °C/min			
ΔH (J/g)	32.57	33.98	35.67	35.91	36.23	36.86
Sdx ($n = 3$)	0.37	0.53	0.20	0.95	0.94	0.45
T_m (°C)	43.30	43.17	43.44	44.76	43.07	43.28
Sdx ($n = 3$)	0.26	0.22	0.18	0.30	0.25	0.10
			1.2 °C/min			
ΔH (J/g)	32.90	33.80	35.72	38.56	36.72	35.79
Sdx ($n = 3$)	0.61	0.65	0.29	0.49	0.89	0.52
T_m (°C)	43.37	42.22	43.48	45.41	43.31	42.84
Sdx ($n = 3$)	0.36	0.48	0.25	0.12	0.41	0.20
			0.4 °C/min			
ΔH (J/g)	27.52	30.93	37.60	36.93	34.72	31.83
Sdx ($n = 3$)	0.25	0.48	0.96	1.19	1.88	0.26
T_m (°C)	42.46	42.87	43.96	44.69	43.76	42.45
Sdx ($n = 3$)	0.25	0.14	0.29	0.34	0.14	0.65

[a]Values represent the average of three replicates ($n = 3$) and the standard deviation of the mean (sdx).

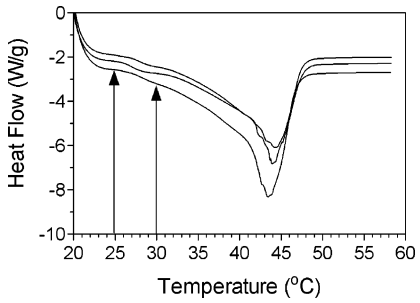

Figure 7. Representative differential scanning calorimetry (DSC) traces of samples crystallized at the three different cooling rates to 20 °C after 1 day of storage at 20 °C.

The increase in oil loss upon exposure to higher maximum cycling temperatures can be explained using DSC as well. As can be appreciated in Figure 6, samples begin to melt at ~25 °C, while the melting process is well under way by 30 °C. Thus, it would stand to reason that the partial melting of samples at 30 °C (Figure 6) would lead to a greater oil loss (Figure 2). No significant trends were detected in the general shape of the melting thermograms, the value of the enthalpy of melting (Table 1), or the position of the peak maxima (Table 1), for samples crystallized at different cooling rates. This was interpreted as samples having the same composition and polymorphic form. Thus, the difference in oil binding capacity for samples crystallized at different cooling rates is not due to differences in composition, or polymorphism, of the fat crystals. This was corroborated by powder X-ray diffraction results (Figure 8). Samples crystallized at 0.4 °C/min (Figure 8A), 1.2 °C (Figure 8B) and 6.0 °C (Figure 8C) were very similar. The small angle reflection at 4.41 nm originates from the 001 plane (the long axis of the unit cell), while the wide angle reflections at 0.42 and 0.38 nm are characteristic of the β' (orthorhombic perpendicular subcell structure) polymorphic form. Thus, the molecular packing of triacylglycerols in the fat crystals was the same for all samples.

Thus, the observed increase in oil binding capacity (Figure 2), elasticity (Figure 3A), and hardness (Figure 4) as a function of increases in the cooling rate experi-

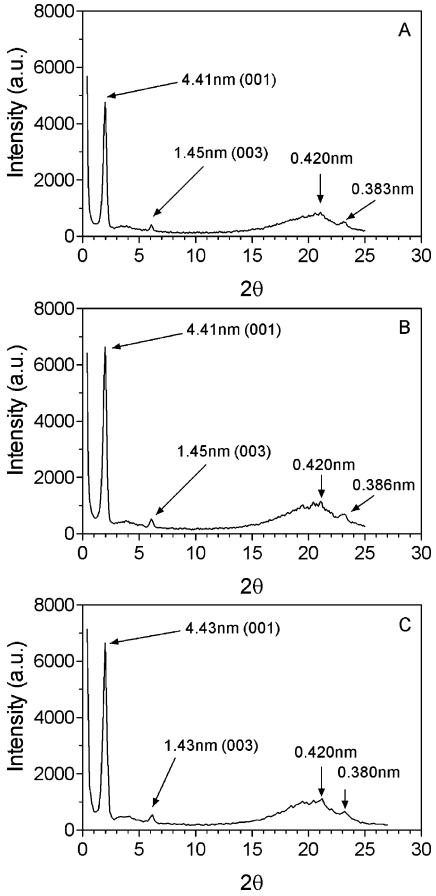

Figure 8. Representative powder X-ray diffraction spectra for samples crystallized at 0.4 °C/min (A), 1.2 °C/min (B), and 6 °C/min (C) to 20 °C after 1 day of storage at 20 °C.

Table 2. Fat Crystal Network Structural Indicators, Calculated Permeability Coefficients (*B*), and Oil Loss Values for Samples Crystallized at the Three Different Cooling Rates to 20 °C after 1 day of Storage at 20 °C[a]

cooling rate (°C/min)	SFC/100	D_b	D_f	α (μm)	B (D_b)	B (D_f)	oil loss (%)
0.4	0.213[a]	1.72[a]	1.99[a]	8.25[a]	760	1490	7.82[a]
1.2	0.236[b]	1.82[b]	1.92[a]	6.76[b]	530	666	2.02[b]
6.0	0.234[b]	1.74[a]	1.99[a]	3.87[c]	150	268	0.023[c]

[a] Values with the same superscript within a column are not significantly different from each other ($p > 0.05$).

enced by the fat mixtures during crystallization, do not seem to be related to differences in polymorphism or composition of the solid state (Table 1 and Figure 8). Moreover, the differences can only be partially explained by the small increase in SFC (Figures 5 and 6).

The microstructure of the samples, on the other hand, was dramatically affected by the cooling rates experienced during crystallization (Figure 9). The average size of crystals (equivalent diameter) decreased with increases in cooling rate (Figure 10). Moreover, the particle counting fractal dimension (D_f) did not change with cooling rate, while the box-counting fractal dimension was higher for 1.2 °C/min relative to 0.4 and 6.0 °C/min, which were not significantly different from each other (Table 2).

On the basis of these findings, it is possible to formulate a hypothesis regarding the effects observed

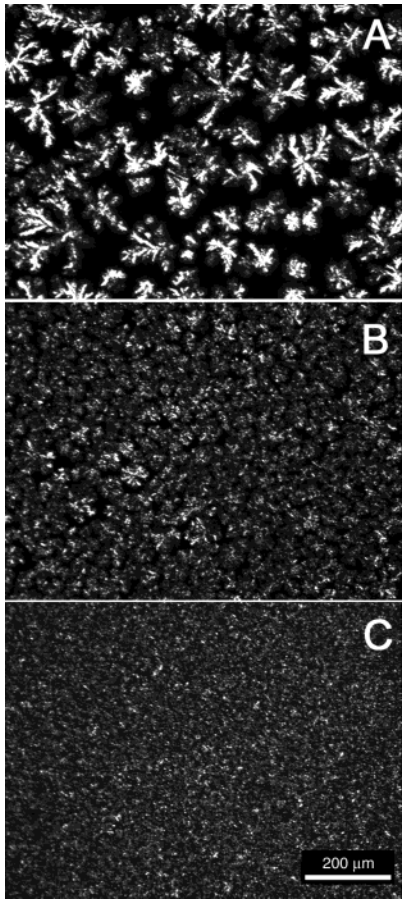

Figure 9. Polarized light micrographs of samples crystallized at 0.4 °C/min (A), 1.2 °C/min (B), and 6 °C/min (C) to 20 °C after 1 day of storage at 20 °C.

Ⓦ Movie files in MPG format to accompany panels Ⓦ A and Ⓦ B are available.

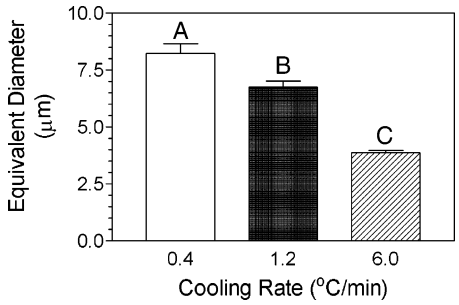

Figure 10. Changes in the average equivalent crystallite diameter of samples crystallized at 0.4 °C/min (A), 1.2 °C/min (B), and 6 °C/min (C) to 20 °C after 1 day of storage at 20 °C.

in light of Darcy's law:

$$Q = \frac{BA_c}{\eta} \cdot \frac{\Delta P}{L} \qquad (2)$$

where Q is the volumetric flow rate, B is the permeability coefficient, A_c is the cross-sectional area through which flow takes place, η is the viscosity of the permeating oil, and ΔP is the pressure drop over the distance L. The permeability coefficient is related to network

structural characteristics, as shown by Bremer et al.:[10]

$$B = \left(\frac{a^2}{K}\right)\Phi^{2/(D-3)} \quad (3)$$

where a is the particle size, K is a parameter comparable to the tortuosity factor in the Kozény-Carman equation, Φ is the solids' volume fraction, and D is the fractal dimension of the network.

This model predicts a higher permeability coefficient with higher fractal dimensions, lower SFC, and larger average particle size. Permeability coefficients were calculated using the structural parameters obtained at 20 °C (Table 2). Two values for B are shown since we have two measures of the fractal dimension. In both cases, it is possible to predict the decrease in permeability coefficient as a function of increases in cooling rate. Focusing on the differences between samples crystallized at 0.4 and 1.2 °C/min, our calculations show a 1.43 (using D_b) or 2.24 (using D_f) times greater permeability coefficient for samples crystallized at 0.4 versus 1.2 °C/min. Oil loss data yielded a value of 3.9 times. The results of the calculations are encouraging since we have not included the contribution of the parameter K in our calculations (see eq 3). When using D_b values in the calculation of the permeability coefficient (B), differences detected are almost exclusively due to changes in particle size. Moreover, oil loss is related to the volumetric flow rate (Q) in eq 2 rather than only the permeability coefficient (B). Thus, the assumption in this analysis is that all parameters in eq 2 remain constant between for the different treatments. This is a reasonable assumption since the geometry and driving force for the oil flow are the same in all cases. The only parameters that could change are the oil viscosity (eq 2) and K (eq 3).

In this work, we have shown the profound effects of cooling rate on oil migration of plastic fats. In our system, these changes were shown to be mainly due to differences in the microstructure of the fat crystal network, specifically average crystal diameter—larger crystals lead to greater oil losses from the network. Polymorphism and crystal composition did not change with cooling rate, while the SFC and fractal dimension did not influence the observed behavior to the same extent that average crystal size did. This work suggests that decreases in oil migration through a semisolid crystalline fat matrix can be engineered by decreasing the size of the crystalline particles.

Acknowledgment. This work was funded by the Natural Sciences and Engineering Research Council of Canada and the Ontario Ministry of Agriculture and Food. Special thanks to Prof. Stefan Idziak and Mr. Gianfranco Mazzanti from the Department of Physics at the University of Waterloo (Canada) for the powder X-ray diffraction analysis, and Ken Baker (Ken Baker Associates) for microscopy support.

Note Added after ASAP Posting

An earlier version of this paper posted to the ASAP website on May 8, 2004, had two temperature values transposed in lines 19 and 20 in the abstract. These have been corrected in this new version posted May 21, 2004.

References

(1) Talbot, G. Fat migration in confectionery products. *Confectionery Prod.* **1989**, *55*, 655−656.
(2) Timms, R. E. *Confectionery Fats Handbook*; The Oily Press: Bridgwater, England, U.K., 2003; pp 255−289.
(3) Miquel, M. E.; Carli, S.; Couzens, P. J.; Wille, H. J.; Hall, L. D. Kinetics of the migration of lipids in composite chocolate measured by magnetic resonance imaging. *Food Res. Int.* **2001**, *34*, 773−781.
(4) Walter, P.; Cornillon, P. Lipid migration in two-phase chocolate systems investigated by NMR and DSC. *Food Res. Int.* **2002**, *35*, 761−767.
(5) Miquel, M. E.; Hall, L. D. Measurement by MRI of storage changes in commercial chocolate confectionery products. *Food Res. Int.* **2002**, *35*, 993−998.
(6) Narine, S. S.; Marangoni, A. G. Relating the structure of fat crystal networks to mechanical properties: a review. *Food Res. Int.* **1999**, *32*, 227−248.
(7) Narine, S. S.; Marangoni, A. G. Structure and mechanical properties of fat crystal networks. *Adv. Food Nutr. Res.* **2002**, *44*, 34−147.
(8) Marangoni, A. G. The nature of fractality in fat crystal networks. *Trends Food Sci. Technol.* **2002**, *13*, 37−47.
(9) Singh, A. P.; Bertoli, C.; Rousset, P.; Marangoni, A. G. By matching Avrami indices it is possible to achieve a similar hardness in palm oil-based fats. *J. Agric. Food Chem.* **2004**, in press.
(10) Bremer, L. G. B.; vanVliet, T.; Walstra, P. Theoretical and experimental study of the fractal nature of the structure of casein gels. *J. Chem. Soc., Faraday Trans. 1* **1989**, *85*, 3359−3372.

CG049933N